Design strategies to tailor the narrow plasmon-photonic resonances in arrays of metallic nanoparticles

T. V. Teperik[1,*] and A. Degiron[1,2]

[1]*Université Paris–Sud, Institut d'Electronique Fondamentale, UMR 8622, F-91405 Orsay, France*

[2]*CNRS Orsay, F-91405 Orsay, France*

(Received 1 July 2012; revised manuscript received 23 October 2012; published 21 December 2012)

Arrays of metallic nanoparticles can support mixed plasmon-photonic resonances known as lattice surface modes. Their properties are well known, but a general strategy to control their properties is still lacking. In this article, we offer a perspective on the formation of these modes and show that their excitation depends on constructive and destructive interferences between the excitation field and the light scattered by the resonant nanoparticles. It is therefore possible to design the response of the system through a careful choice of the excitation conditions and/or by tuning the polarizability of the particles forming the periodic arrays.

DOI: 10.1103/PhysRevB.86.245425 PACS number(s): 42.25.Fx, 73.20.Mf, 78.66.Bz, 78.67.−n

I. INTRODUCTION

Noble metal nanoparticles have been the subject of a tremendous number of studies due to their ability to sustain localized surface plasmon resonances (LSPRs) that confine light at a deep subwavelength scale. These resonances can be tuned from the infrared to the visible region by a careful choice of the geometry, metal, and dielectric environment.[1–3] Their linewidth and spectral shape can also be controlled by making nanoparticles interact, leading to the formation of dark and bright coupled modes with typical Fano profiles.[4] This rich optical behavior plays a central role in many fields of optics, including miniaturized sensors, near-field microscopy, solar energy harvesting, optical metamaterials, and the manipulation of light produced by molecules and quantum dots.

In addition to LSPRs, metal nanoparticles also support collective modes when they are arranged into a periodic lattice. It is known that such *plasmonic crystals* support a collective resonance that is broadened and blueshifted or redshifted with respect to the resonance of an isolated particle.[5] Also intriguing is the fact that certain arrays support a mixed *plasmon-photonic* resonance that results from the coupling between the diffractive Rayleigh anomalies and the individual LSPRs of the particles. This resonance is the so-called lattice surface mode (LSM) that propagates along the lattice and is characterized by extremely narrow line shapes in extinction and scattering. The existence of LSMs was first reported for an array of silver nanoparticles in the context of plasmon enhanced Raman scattering from absorbed molecules.[6] The potential of this narrow mode for biosensing applications has been highlighted by several studies,[7–10] and LSMs have also been discussed in the context of thermal emission and resonant absorption.[11] Nowadays, we observe a renewed interest in this phenomenon,[10,12–15] and more especially in the context of the spontaneous emission of plasmonic nanostructures.[16–18] It is worth noting that purely *photonic* LSMs have also been theoretically predicted for periodic lattices of dielectric cylinders,[19,20] dielectric spheres,[21,22] and perfectly conducting disks,[23] as well as for hole arrays in a perfectly conducting screen.[24]

While LSMs have been discussed in many theoretical and experimental studies, one can still wonder what is the best strategy to observe and tune these resonances. In this article, we argue that controlling the illumination conditions and tailoring the polarizability of the individual particles are two powerful means to control the optical properties of LSMs.

II. ELECTROMAGNETIC MODEL AND BASIC EQUATIONS

We briefly recall the theory of LSMs for an infinite array of metallic nanoparticles illuminated by a plane wave. This system can be conveniently modeled using the coupled dipole (CD) method[7–9,13,23,25] when the particles are small compared to both the wavelength and their separation. Within the framework of the CD method, the details of which can be found in a tutorial review,[23] a particle at position $\mathbf{R}_n = (x_n, y_n, z = 0)$ is characterized by an electric polarizability α and responds to the local field $\mathbf{E}_{\rm loc}$ with an induced dipole

$$\mathbf{p}_n = \varepsilon_0 \alpha \mathbf{E}_{\rm loc}(\mathbf{R}_n), \tag{1}$$

where ε_0 is the permittivity in vacuum. The local field acting on a particle $\mathbf{E}_{\rm loc}$ consists of the incident field $\mathbf{E}_{\rm inc}$ and the retarded field of other particles that can be expressed in terms of the dipole-dipole interaction tensor as $\omega^2\mu_0 \sum_{n'\neq n} \overleftrightarrow{G}(\mathbf{R}_n - \mathbf{R}_{n'})\mathbf{p}_{n'}$. Here $\overleftrightarrow{G}(\mathbf{R}_n - \mathbf{R}_{n'})$ is the diadic Green function and μ_0 is the permeability in vacuum. With these elements, Eq. (1) becomes

$$\mathbf{p}_n = \alpha\varepsilon_0 \mathbf{E}_{\rm inc} + \alpha k^2 \sum_{n'\neq n} \overleftrightarrow{G}(\mathbf{R}_n - \mathbf{R}_{n'})\mathbf{p}_{n'}, \tag{2}$$

with $k = \omega\sqrt{\varepsilon_0\mu_0}$. For a plane wave illuminating the lattice at normal incidence with an electric field parallel to the x axis, $\mathbf{E}_{\rm inc} = e^{-ikz}\hat{\mathbf{x}}$, the polarization of a particle is $\mathbf{p}_n = p\hat{\mathbf{x}}$, so the induced dipole of each particle takes the form[9]

$$p = \frac{\varepsilon_0}{1/\alpha - S}, \tag{3}$$

where $S = k^2 \sum_{n'\neq n} G_{xx}(\mathbf{R}_n - \mathbf{R}_{n'})$ is the retarded dipole sum, $G_{xx}(\mathbf{r} - \mathbf{r}') = [1 + \frac{1}{k^2}\frac{\partial^2}{\partial x^2}]g(\mathbf{r} - \mathbf{r}')$ is the first diagonal element of the Green's tensor,[26] and $g(\mathbf{r} - \mathbf{r}')$ is the scalar Green's function. It is very useful to use the plane-wave decomposition of $g(\mathbf{r} - \mathbf{r}')$ (Ref. 27) to represent the sum S.

Using this strategy, we obtain the following expression for S:

$$S = \frac{i}{2}\lim_{z\to 0}\left\{\frac{1}{a^2}\sum_{\mathbf{g}}\frac{e^{iq_z|z|}\left(k^2-g_x^2\right)}{g_z} - \frac{1}{4\pi^2}\int dq_x\,dq_y\,\frac{e^{iq_z|z|}\left(k^2-q_x^2\right)}{q_z}\right\}. \quad (4)$$

Here a is the lattice constant, $\mathbf{g} = (g_x, g_y)$ are the reciprocal-lattice vectors, $g_z = \sqrt{k^2 - g_x^2 - g_y^2}$, and $q_z = \sqrt{k^2 - q_x^2 - q_y^2}$. The integral in Eq. (4) represents the substraction of the $n' = n$ term in the sum S. It can be seen that this integral is actually the plane-wave decomposition of a single dipole field and can be calculated directly in real space. Thus, the sum S can be rewritten as

$$S = \frac{1}{2}\lim_{z\to 0}\left\{\frac{i}{a^2}\sum_{\mathbf{g}}\frac{e^{iq_z|z|}\left(k^2-g_x^2\right)}{g_z} - \frac{e^{ik|z|}}{2\pi|z|^3}\left[(kz)^2 + ik|z| - 1\right]\right\}. \quad (5)$$

Once the induced dipole is obtained, the field scattered from the lattice of particles is calculated as a sum of the electromagnetic field produced by the lattice of dipoles with induced dipole moments $\mathbf{p} = p\hat{\mathbf{x}}$. The reflection and transmission coefficients are

$$R = |r_0|^2\sum_{\mathbf{g}}\frac{k^2-g_x^2}{kq_z}, \qquad T = R + |1+r_0|^2 - |r_0|^2, \quad (6)$$

where $r_0 = ik/[2a^2(1/\alpha - S)]$ and the sum of Eq. (6) is taken only over the open diffractive channels when $k^2 > g_x^2 + g_y^2$. The absorption can be calculated as $A = 1 - R - T$.

Variants of these equations have been obtained and discussed by several articles in the past.[7–9,13,23] The resonances of the system are given by the zeros of the denominator of r_0, which shows that the contributions of the lattice (S) and of the particles (α) are separated. The properties of the sum S are also known: it diverges at Rayleigh anomalies ($k^2 = q_x^2 + q_y^2$) that are associated with the opening of new diffraction orders in surrounding media. The polarizability α can be calculated with analytical or numerical approaches depending on the size and geometry of the particles. For small spheres, ellipsoids, cylinders, and disks, it is generally sufficient to calculate α analytically in the electrostatic limit,[28] but the result should be amended by a radiation-damping correction.[29,30] Another way to calculate the polarizability is to use the Mie theory through the scattering matrix coefficients.[31,32] In the latter case, the resulting polarizability accounts for radiative damping and can be used for larger particles when the electrostatic approximation fails. For more complicated structures, purely numerical methods are needed. In this article, we calculate the polarizability α using the boundary element method.[33] More precisely, we compute the electric far-field induced by a single particle illuminated with the incident electric field $\mathbf{E}_{\text{inc}} = e^{-ikz}\hat{\mathbf{x}}$. Then, assuming that the contribution of the dipole mode is dominant, we extract the dipolar moment and polarizability of the particle.

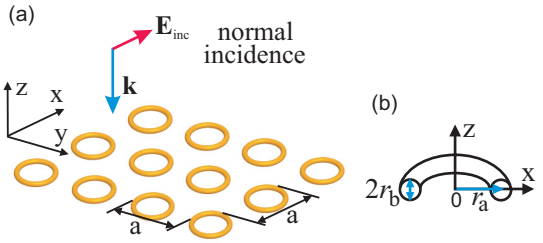

FIG. 1. (Color online) (a) Schematic of the square array of nanorings illuminated by a plane wave. (b) Geometry of the Au rings.

III. TAILORING LSMs WITH THE INCIDENT FIELD

We begin our study by considering an infinite array of Au nanorings illuminated with a plane wave at normal incidence (see Fig. 1). Such particles possess highly tunable plasmonic resonances in the visible and near infrared.[34–36] Figures 2(a) and 2(d) present the calculations of Re(α) as a function of the wavelength for two individual rings with radius $r_a = 60$ and 90 nm, respectively. We observe that the polarizability exhibits a resonant behavior associated with the excitation of the fundamental plasmon resonance of the ring. The polarizability of a subwavelength plasmonic nanoring has a Lorentzian form $\alpha = -A/(\omega - \omega_r + i\gamma)$, where A is a positive real constant, ω_r is the frequency of the plasmon resonance for the isolated particle, and γ is its half-width due to dissipative and radiative damping. Thus, the resonant wavelength of a single ring is given by Re$(1/\alpha) = 0$. The plasmon resonance of a nanoring is extremely sensitive to its size and shifts by 310 nm to the blue by reducing the ring's radius from 90 to 60 nm.

The collective resonances of the periodic arrays based on these two ring geometries are discussed in the remaining panels of Fig. 2. To analyze the resonant denominator in Eq. (3), we have calculated separately the real parts of the lattice sum Re(S) and inverse polarizability Re$(1/\alpha)$, as well as the imaginary part of the denominator in Eq. (3), Im$(1/\alpha - S)$; see Figs. 2(b) and 2(e). As expected, the lattice sum diverges at the diffraction (Rayleigh) thresholds; for a square lattice in vacuum, their position is given by $\lambda = 2\pi/\sqrt{g_x^2 + g_y^2}$, i.e., $\lambda = a$ and $\lambda = a/\sqrt{2}$. At these positions, the imaginary part of the denominator Im$(1/\alpha - S)$ exhibits a jump. The same phenomenon has been reported in Ref. 32 for a chain of spherical plasmonic particles.

In Figs. 2(c) and 2(f), we present the transmission spectra through the two structures calculated from Eq. (6). In addition to CD model calculations [using Eq. (6)], we also show the transmission obtained rigorously within the framework of a multiple-scattering layer Korringa-Kohn-Rostoker (KKR) approach,[37,38] where the scattering matrix of a ring has been calculated separately with the boundary element method (BEM).[33] This combined method includes a converged multipole expansion on each particle. One can observe a good quantitative agreement between the model and the rigorous calculations (for small rings the discrepancy at resonance is less than 1%), supporting our assumption about the dominant dipole response of a nanoring.

The transmission spectra exhibit several resonances corresponding to the condition Re$(1/\alpha - S) = 0$. The broad minima at 890 and 1200 nm in Figs. 2(c) and 2(f), respectively,

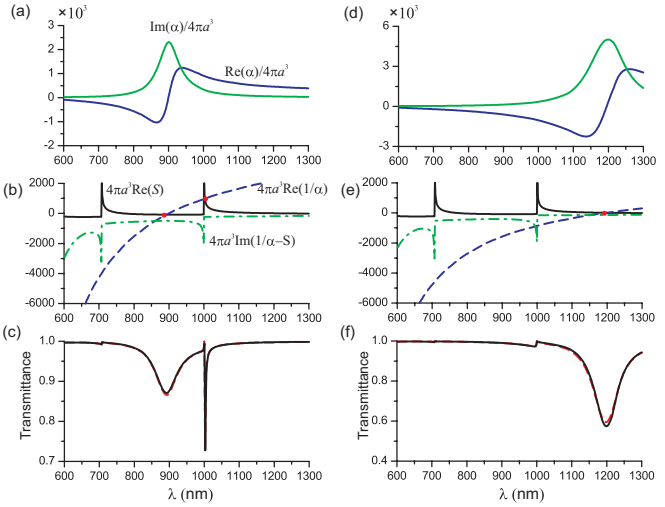

FIG. 2. (Color online) (a) Wavelength dependence of the real (blue curve) and imaginary parts (green curve) of the resonant polarizability α for Au rings with radius $r_a = 60$ nm and thickness $2r_b = 25$ nm. (b) Wavelength dependence of $\mathrm{Re}(1/\alpha)$ (blue dashed curve), $\mathrm{Re}(S)$ (black curve), and the imaginary part of the denominator of Eq. (3) (green dashed-dotted curve) when the Au rings form a periodic structure with a lattice constant $a = 1000$ nm. (c) Normal-incidence transmission spectrum of the structure: CD model calculations (black curve) and multiple-scattering approach (red dashed curve). (d,e,f) Same as (a,b,c), except that the ring radius is $r_a = 90$ nm. Plots (a,b,d,e) are normalized to $4\pi a^3$.

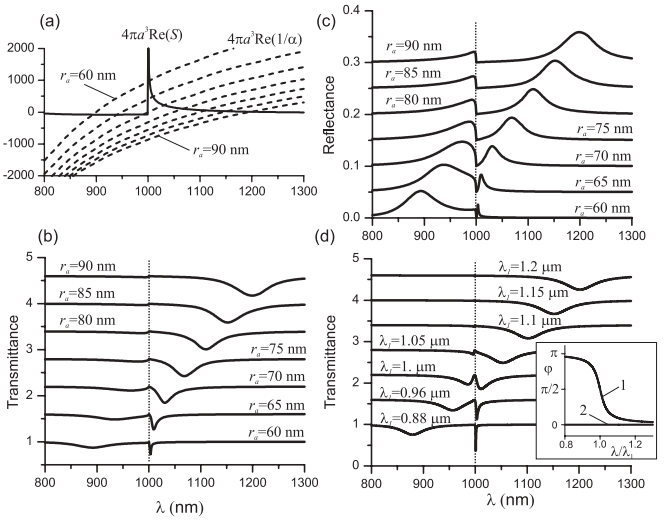

FIG. 3. (a) Wavelength dependence of $\mathrm{Re}(1/\alpha)$ (dashed curve) and $\mathrm{Re}(S)$ (solid curve) for plasmonic crystals with ring radii varying from $r_a = 90$ to 60 nm with a 5 nm step. The ring thickness is $2r_b = 25$ nm in all cases and the curves are normalized to $4\pi a^3$ ($a = 1000$ nm). (b) Transmittance and (c) reflectance spectra at normal incidence. (d) Transmission spectra according to the generic oscillator model described by Eqs. (7a) and (7b) for different values of $\lambda_1 = 2\pi c/\omega_1$ as indicated on the graph. Here the transmission is defined as $1 - A$, where $A = a_1\dot{x}_1 + a_2\dot{x}_2$ represents the absorption of excitations 1 and 2 by oscillators 1 and 2, respectively. The curves are vertically offset for clarity. Inset: Relative phase of oscillator 1 (curve 1) and relative phase of excitation $a_2 \exp(i\omega t)$ (curve 2).

are associated with the excitation of the plasmon resonances localized on the rings. Since S is small at these wavelengths, the position of these peaks are close to the resonant condition $\mathrm{Re}(1/\alpha) = 0$ of a single ring. The sharp asymmetrical dip seen in Fig. 2(c) is associated with the excitation of the lattice surface mode that propagates along the lattice. It is characterized by a narrow but nonzero width[8] associated with the imaginary part of the denominator $\mathrm{Im}(1/\alpha - S)$. This mode is only observed in the spectra of the structure with the smallest rings and corresponds to the intersection of the $\mathrm{Re}(1/\alpha)$ curve with the diffractive anomaly of $\mathrm{Re}(S)$ in Fig. 2(b). As already noted by others,[6,7,10,12,13,39] this condition only occurs when the localized plasmon resonance is blueshifted with respect to a given Rayleigh anomaly. When the localized surface plasmon resonance is on the red side of the Rayleigh thresholds, the lattice surface mode cannot be excited and only small dips are visible in the transmission spectra at these wavelengths; see Fig. 2(f).

To understand how the LSM modes can be tailored in a systematic way, we note that the salient features of Fig. 2 are those of a broad, low-quality factor resonance that interacts with a much narrower one. Thus, we are dealing with Fano resonances, and their properties can be emulated with a system of two coupled harmonic oscillators:[40]

$$\ddot{x}_1 + \gamma_1\dot{x}_1 + \omega_1^2 x_1 + \kappa_{12}^2 x_2 = a_1 e^{i\omega t}, \tag{7a}$$

$$\ddot{x}_2 + \gamma_2\dot{x}_2 + \omega_2^2 x_2 + \kappa_{12}^2 x_1 = a_2 e^{i\omega t}, \tag{7b}$$

where x_1 and x_2 describe the movement of the low- and high-Q oscillators, respectively, $\gamma_1 \gg \gamma_2$ are their damping factor, ω_1 and ω_2 are their eigenfrequencies, and κ_{12} is the coupling coefficient. The oscillators are driven by two excitation sources $a_1 \exp(i\omega t)$ and $a_2 \exp(i\omega t)$ to account for the fact that the diffractive Rayleigh anomaly can be excited independently from the localized surface plasmon resonance due to the sole periodicity of the system.

The importance of driving both oscillators can be illustrated by exploring how the transmission spectrum evolves as the localized surface plasmon resonance moves through the Rayleigh anomaly. Figures 3(a) and 3(b) represent the results of the transmission and reflection calculations given by Eq. (6) when the size of the rings decreases from 90 to 60 nm, while Fig. 3(d) shows the predictions given by the modified coupled oscillator model. In the later case, the calculations have been performed with excitations $a_1 = 8$, $a_2 = 0.8$, a Rayleigh anomaly with an angular frequency $\omega_2 = 2\pi\ 300 \times 10^{12}$ rad s^{-1} (i.e., a resonance wavelength $\lambda_2 = 1000$ nm), a coupling factor $\kappa_{12} = 295 \times 10^{12}$ rad s^{-1}, and the losses have been set to $\gamma_1 = 0.06\omega_1$ and $\gamma_2 = 0.8 \times 10^{12}$ rad s^{-1}, respectively. With these parameters, the simple oscillator model successively reproduces the transmission curves of the nanoring array; in particular, the LSM appears only after the localized surface plasmon has passed from the red to the blue side of the Rayleigh anomaly and its width becomes narrower and narrower as the localized plasmon shifts to smaller wavelengths.

The parameters used to generate the curves of Fig. 3(d) provide valuable insight into the system and how LSMs can be tuned using the external field. In this graph, the plasmon resonance (i.e., the lossy resonator) must be driven by a source with an amplitude a_1 roughly 10 times higher than a_2 to reproduce the electromagnetic calculations of Fig. 3(b). Under

such conditions, the Rayleigh anomaly (represented by the second oscillator) is excited by two sources of nearly equivalent strength—the incoming excitation $a_2 \exp(i\omega t)$ and the localized plasmon resonance through the coupling parameter κ_{12}. To understand the influence of these two contributions on the Rayleigh anomaly, we have plotted their relative phase as a function of the wavelength in the inset of Fig. 3(d). By definition, the relative phase of $a_2 \exp(i\omega t)$ is always equal to zero while the phase of the uncoupled surface plasmon resonance is that of a damped harmonic oscillator and therefore rapidly shifts from 0 to π in the vicinity of the plasmon resonance $\lambda_1 = 2\pi c/\omega_1$. When the surface plasmon is on the blue side of the Rayleigh anomaly, it excites this resonance with the same phase as $a_2 \exp(i\omega t)$ and therefore the two excitations interfere constructively to form the LSM mode. The opposite is true when the localized surface plasmon is on the red side of the Rayleigh anomaly: in this case, the surface plasmon is π-shifted and negatively interferes with the incoming light, preventing the formation of the LSM.

Thus, the excitation of LSMs depends on a subtle interplay between the incoming field and the light scattered by the nanoparticles. This conclusion implies that the formation of LSMs can be tuned by tailoring the structure of the incident field itself. In particular, it is possible to find configurations where LSMs are excited when the localized surface plasmon is on either side of the Rayleigh anomaly, for example if the rings are coupled to a lattice of coherent point-source emitters.[41] In contrast to the plane-wave illumination considered in this section, coherent emitters contribute strongly to the Rayleigh anomaly, so the destructive interferences caused by the phase of the localized surface plasmon resonance are not strong enough to cancel out the formation of LSMs.

IV. TAILORING LSMs WITH THE POLARIZABILITY OF THE PARTICLES

Having discussed the role of the excitation conditions, we now investigate how LSMs can be tuned with the different parameters defining the system. It is well documented in the literature that the LSM excitation conditions can be controlled by the particle volume, particle form, periodicity, filling factor, and type of metal. From Eq. (3) we see that these parameters act upon two factors—the dipole sum S and the individual particle polarizability α. As we know,[9] the dipole sum S is a purely geometrical factor, while all the other properties are essentially defined by α. This point can be discussed in more detail by examining the transition between large and small rings in Figs. 3(a) and 3(b). As the ring radius decreases, the inverse polarizability $\mathrm{Re}(1/\alpha)$ passes through the first Rayleigh anomaly of the S curve [Fig. 3(a)], generating a splitting of the transmission resonance for ring radii smaller than 70 nm [Figs. 3(b) and 3(c)]. This splitting is of course the signature of the coupling between the localized plasmon resonance and the Rayleigh anomaly. The strength of the coupling is given by the gap between the two modes at the anticrossing point. As shown in Fig. 3(a), this gap can be controlled by the slope of the inverse polarizability $\mathrm{Re}(1/\alpha)$—for particles with inverse polarizabilities that are flatter than those shown here, the anticrossing would be larger because the intersection points between the $\mathrm{Re}(1/\alpha)$ and the

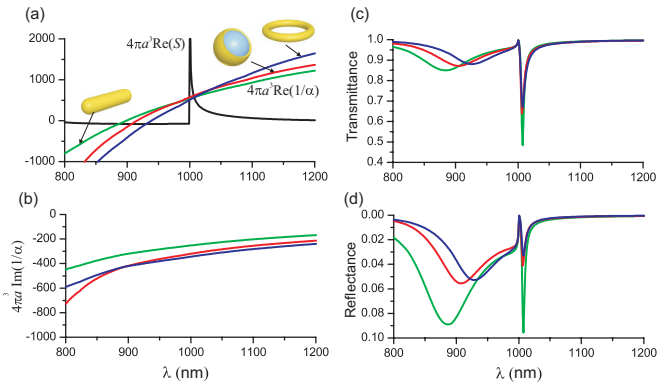

FIG. 4. (Color online) (a) Wavelength dependence of $\mathrm{Re}(S)$ (black curve) and $\mathrm{Re}(1/\alpha)$ for three nanoparticle arrays with the same period $a = 1000$ nm. Blue curve: Au rings with radius and thickness equal to 64 and 25 nm, respectively; red curve: Au shells with a core of SiO_2 and inner and outer radii equal to 70 and 75 nm, respectively; green curve: Au rods with length and thickness equal to 182 and 20 nm. The curves are normalized to $4\pi a^3$. (b) Wavelength dependence of $\mathrm{Im}(1/\alpha)$ for the three types of particles. (c) and (d) Transmittance and reflectance spectra for the three arrays.

S curves would be set farther apart. Note that gaining control over the anticrossing point provides an opportunity to change the lifetime of both the surface plasmon resonance and the LSM because of the mixing of the two modes in this region.

The extent to which the inverse polarizability $\mathrm{Re}(1/\alpha)$ of individual nanoparticles can be tuned depends on how many geometrical and material parameters (e.g., particle form/shape, permittivity, and environment) are accessible in practice. Generally, these different contributions are interdependent, complicating the design of the structures. This behavior is apparent in Fig. 3(a), where it can be seen that reducing the size of the rings not only shifts the $\mathrm{Re}(1/\alpha)$ curve but also makes it steeper because of the dispersion of Au. To modify the slope of $\mathrm{Re}(1/\alpha)$, it is necessary to replace the Au rings with nanoparticles having approximately the same resonance wavelength but other scattering properties.

Figure 4 illustrates this point by presenting the optical properties of plasmonic crystals made of Au rings, Au nanorods, and Au nanoshells with a SiO_2 core, respectively. All three particles are highly tunable because of their relatively complex geometry. In this example, we adjusted their dimensions and aspect ratio so that their inverse polarizability $\mathrm{Re}(1/\alpha)$ crosses the peak of the lattice sum $\mathrm{Re}(S)$ at the same wavelength [Fig. 4(a)]. As expected, this condition ensures that the LSMs supported by the different arrays have the same spectral position; see the transmission and reflection spectra of Figs. 4(c) and 4(d). In contrast, the broad localized plasmon resonances are positioned at very different wavelengths (926, 905, and 884 nm for nanorings, nanoshells, and nanorods, respectively) and their width and shape also vary. This behavior arises because the three types of particles interact with light differently; their inverse polarizabilities have distinct slopes and therefore the localized plasmon resonance condition is not satisfied at the same wavelengths. One can see that the strength of the LSMs is directly related to the losses, and more precisely to the absorption properties of the individual particles, because all three arrays have the same period. Figure 4(b) plots

the imaginary part of the inverse polarizability of the three different nanoparticles and shows that the rods have the smallest material losses in this wavelength range, leading to the strongest resonance.

Similar spectral changes can also be obtained by modifying the permittivity of the nanoparticles rather than their geometry. For example, the localized plasmon resonance of the ring array of Fig. 4 can be blueshifted by about 50 nm by working with Ag rather than Au (results not shown here). Thus, several levers are readily at hand to tune the optical response of particle arrays, and these different approaches may be combined to optimize the design of a given structure.

V. CONCLUSIONS

The narrow plasmon-photonic resonances associated with the excitation of lattice surface modes in nanoparticle arrays can be tuned with great flexibility by tailoring the excitation condition and by engineering the polarizability of the particles. We have discussed the influence of the polarizability for lattices of plasmonic nanorings, nanoshells, and nanorods, and this conclusion can be extrapolated for other structures as well. Since the polarizability is directly related to the metal properties, the environment, the dimensions, and the shape of the particles, it is preferable to consider relatively complex geometries because they offer more degrees of freedom for tuning the resonant properties of the system.

ACKNOWLEDGMENTS

We would like to thank Andrey G. Borisov for stimulating discussions. Financial support for this work was provided by the RTRA Triangle de la Physique under Grant No. 2010-008T.

*tatiana.teperik@u-psud.fr

[1] S. Lal, S. Link, and N. J. Halas, Nat. Photon. **1**, 641 (2007).
[2] J. Kottmann, O. J. F. Martin, D. R. Smith, and S. Schultz, Opt. Express **6**, 213 (2000).
[3] K. L. Kelly, E. Coronado, L. L. Zhao, and G. C. Schatz, J. Phys. Chem. B **107**, 668 (2003).
[4] B. Luk'yanchuk, N. I. Zheludev, S. A. Maier, N. J. Halas, P. Nordlander, H. Giessen, and C. T. Chong, Nat. Mater. **9**, 707 (2010).
[5] L. Zhao, K. L. Kelly, and G. C. Schatz, J. Phys. Chem. B **107**, 7343 (2003).
[6] K. T. Carron, W. Fluhr, M. Meier, A. Wokaun, and H. W. Lehmann, J. Opt. Soc. Am. B **3**, 430 (1986).
[7] S. Zou, N. Janel, and G. C. Schatz, J. Chem. Phys. **120**, 10871 (2004).
[8] V. A. Markel, J. Chem. Phys. **122**, 097101 (2005).
[9] S. Zou and G. C. Schatz, J. Chem. Phys. **122**, 097102 (2005).
[10] P. Offermans, M. C. Schaafsma, S. R. K. Rodriguez, Y. Zhang, M. Crego-Calama, S. H. Brongersma, and J. Gómez Rivas, ACS Nano **5**, 5151 (2011).
[11] M. Laroche, S. Albaladejo, R. Gómez-Medina, and J. J. Sáenz, Phys. Rev. B **74**, 245422 (2006).
[12] Y. Chu, E. Schonbrun, T. Yang, and K. B. Crozier, Appl. Phys. Lett. **93**, 181108 (2008).
[13] B. Auguié and W. L. Barnes, Phys. Rev. Lett. **101**, 143902 (2008).
[14] V. G. Kravets, F. Schedin, and A. N. Grigorenko, Phys. Rev. Lett. **101**, 087403 (2008).
[15] S. R. K. Rodriguez, A. Abass, B. Maes, O. T. A. Janssen, G. Vecchi, and J. Gómez Rivas, Phys. Rev. X **1**, 021019 (2011).
[16] V. Giannini, G. Vecchi, and J. Gómez Rivas, Phys. Rev. Lett. **105**, 266801 (2010).
[17] G. Vecchi, V. Giannini, and J. Gómez Rivas, Phys. Rev. Lett. **102**, 146807 (2009).
[18] S. Rodriguez, G. Lozano, M. A. Verschuuren, R. Gomes, K. Lambert, B. De Geyter, A. Hassinen, D. Van Thourhout, Z. Hens, and J. Gómez Rivas, Appl. Rev. Lett. **100**, 111103 (2012).
[19] A. G. Borisov and S. V. Shabanov, J. Comput. Phys. **209**, 643 (2005).
[20] R. Gómez-Medina, M. Laroche, and J.-J. Sáenz, Opt. Express **14**, 3730 (2006).
[21] G. Pellegrini, G. Mattei, and P. Mazzoldi, ACS Nano **3**, 2715 (2009).
[22] R. Sainidou, J. Renger, T. V. Teperik, M. U. González, R. Quidant, and F. G. García de Abajo, Nano Lett. **10**, 4450 (2010).
[23] F. J. García de Abajo, Rev. Mod. Phys. **79**, 1267 (2007).
[24] F. J. García de Abajo, R. Gómez-Medina, and J. J. Sáenz, Phys. Rev. E **72**, 016608 (2005).
[25] B. Auguié, X. M. Bendaña, W. L. Barnes, and F. J. García de Abajo, Phys. Rev. B **82**, 155447 (2010).
[26] L. Novotny and B. Hecht, *Principles of Nano-Optics* (Cambridge University Press, Cambridge, 2006).
[27] L. A. Blanco and F. J. García de Abajo, Phys. Rev. B **69**, 205414 (2004).
[28] C. Bohren and D. Hufmann, *Absorption and Scattering of Light by Small Particles* (Wiley, New York, 1998).
[29] B. T. Draine, Astrophys. J. **333**, 848 (1988).
[30] R. Carminati, J.-J. Greffet, C. Henkel, and J. M. Vigoureux, Opt. Commun. **261**, 368 (2006).
[31] W. T. Doyle, Phys. Rev. B **39**, 9852 (1989).
[32] V. A. Markel, J. Phys. B **38**, L115 (2005).
[33] F. J. García de Abajo and A. Howie, Phys. Rev. B **65**, 115418 (2002).
[34] J. Aizpurua, P. Hanarp, D. S. Sutherland, M. Käll, G. W. Bryant, and F. J. García de Abajo, Phys. Rev. Lett. **90**, 057401 (2003).
[35] A. Mary, D. M. Koller, A. Hohenau, J. R. Krenn, A. Bouhelier, and A. Dereux, Phys. Rev. B **76**, 245422 (2007).
[36] T. V. Teperik and A. Degiron, Phys. Rev. B **83**, 245408 (2011).
[37] N. Stefanou, V. Yannopapas, and A. Modinos, Comput. Phys. Commun. **113**, 49 (1998).
[38] F. J. García de Abajo, Phys. Rev. Lett. **82**, 2776 (1999).
[39] E. M. Hicks, S. Zou, G. C. Schatz, K. G. Spears, R. P. Van Duyne, L. Gunnarsson, T. Rindzevicius, B. Kasemo, and M. Käll, Nano Lett. **5**, 1065 (2005).
[40] Y. S. Joe, A. M. Satanin, and C. S. Kim, Phys. Scr. **74**, 259 (2006).
[41] T. V. Teperik and A. Degiron, Phys. Rev. Lett. **108**, 147401 (2012).